

A DISCRETE FORMULATION APPLIED TO CRACK GROWTH PROBLEMS

A. Nappi, S. Rajgelj and D. Zaccaria

Dept. of Civil Engineering, University of Trieste, P.le Europa 1, 34127 Trieste, Italy

Abstract

The paper is centred on a *direct discrete* approach, applicable to a large class of physical problems. Structural systems are considered and the governing equations are derived in a discrete form without using a differential formulation. The numerical technique is similar to the finite volume method and requires the use of two meshes: one to properly describe the distribution of configuration variables (displacements), one to enforce equilibrium. A discrete number of potential crack paths is provided by the second mesh and fracture processes are studied by introducing a proper criterion. The general features of the method are pointed out by considering general problems related to quasi-brittle fracture and by discussing applications to masonry.

Introduction

A discrete formulation is presented which is suitable for the numerical solution of mechanical problems (both linear and nonlinear). Possible applications to cracking phenomena are proposed by exploiting the particular pattern of a mesh, that is typical of the numerical approach and provides a discrete number of paths along which cracks may propagate. Plane structural systems are considered, but the methodology is applicable to more general cases.

The first part of the paper gives general information on the theoretical background and on the fundamental feature of the method: a clear distinction between the different roles played by *configuration variables* and *source variables*. In this way we follow the layout suggested by the scheme known as *Tonti Diagram* [1, 2, 3] or *Generalised Tonti Diagram* [4], that is applicable to a large class of physical problems, such as heat transfer, fluid dynamics, elasticity and electromagnetism [5]. It is shown that two different meshes can be defined by keeping configuration variables (*e.g.*, temperature, electric potential, displacements) separate from source variables (*e.g.*, heat production, electric charge, forces). In the case of structural problems a first (*primal*) mesh allows one to derive compatibility equations, while a second (*dual*) mesh is utilised to enforce equilibrium. It should be noted that discrete governing equations are directly obtained: no intermediate differential formulations are considered before recovering the discrete form needed for numerical applications.

Next, the dual mesh and its possible use in the context of fracture processes are discussed. By means of the dual mesh the continuum is subdivided into a number of relatively small polygons, for which balance (equilibrium) equations are written. To this aim, the total contribution of the loads acting on each polygon (body forces and tractions along the polygon sides) is set equal to zero. Traction are due to external surface loads or to forces exchanged with the remaining part of the continuum. At this stage it is noted that the polygon sides (altogether) provide a discrete number of *zig-zag paths*, since the interface course tends to turn left and right, up and down, repeatedly in a sharp way. Therefore, interfaces can be recognised as potential crack paths and a convenient criterion can be introduced in order to define critical loads beyond which cracks start to propagate. For instance, Coulomb's yield condition or Barenblatt's cohesive model may be considered [6, 7].

Finally, some numerical examples are presented. First, macroscopically homogeneous systems made of quasi-brittle materials are dealt with. Next, applications to masonry structures are briefly discussed [8].

The cell method: primal and dual mesh

We start by considering any portion of a plane structural system subdivided into triangular *primal cells*. An example is given in Fig. 1, where primal cells are shown by thick lines. This kind of cell complex is usually called *simplicial complex*, since it consists of triangular cells or *simplexes*. The values attained by the configuration variables at the vertices of each triangle can be used in order to define their distribution inside the cell. Because of this choice, a linear displacement field is assumed inside the triangle. However, higher order distributions may also be selected [9].

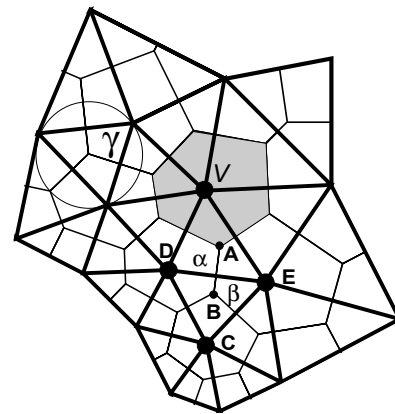


Fig. 1 - Primal and dual mesh

Next, we need to describe the flow of some physical quantities through proper interfaces. One possible choice is the interface *AB* (Fig. 1) along the axis of the segment *DE*. Indeed, the interface is located between two points (the vertices *D* and *E*), where a significant parameter is evaluated. For instance, if we are dealing with heat flow, its value through *AB* can be related to the temperatures at *D* and *E*. Alternatively, for typical problems found in the context of solid mechanics we can consider the force along *AB*: its value depends upon the displacements at *C*, *D*, *E* and *V*. The points *A* and *B* may be the circumcentres of the cells α and β . By properly connecting all the circumcentres of the triangles, polygons or *dual cells* (such as the shaded area in Fig. 1) are defined. At this stage, a balance equation (equilibrium equation in solid mechanics) can be written by taking into account inward flows, outward flows and possible sources concerned with a given cell (*e.g.*, the cell around *V* in Fig. 1).

Thus, a pair of dual meshes will be used: one for configuration variables (and, hence, for compatibility equations in solid mechanics), one for source variables (and, hence, for equilibrium equations). However, we need to investigate dual cells and related properties a bit further. Indeed, we should know (and avoid) possible situations that imply circumcentre locations which are not suitable for a correct evaluation of physical quantities. One undesired situation occurs if two circumcentres are coincident (as it happens with two right-angled triangles whose interface is their hypotenuse). Further

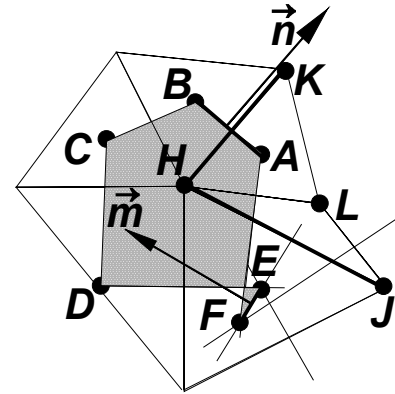


Fig. 2 - Inward and outward flows

problems would arise with primal cells such as the ones presented in Fig. 2 and characterised by the obtuse-angled triangle HJL . Indeed, if we refer again to heat transfer problems, we note that each side of the primal mesh (e.g., HK) must be associated to an outward unit vector \mathbf{n} (oriented from H to K). Then, an equation based on this vector would imply a heat flow through AB featuring the same orientation of \mathbf{n} when the temperature at H is higher. If we move along the axes of the other segments centred around H , we obviously expect consistent orientations (i.e., unit vectors oriented from the left to the right as we go from B to C , from C to D , and so on). Thus, the vector \mathbf{m} should be oriented as shown in Fig. 2. Its orientation would give a relationship that implies a heat flow through EF from J to H if the temperature at J is lower. Obviously, this is not consistent with the physical phenomenon. In addition, a polygon such as $ABCDEF$ does not allow one to give a clear meaning to the concept of inward/outward flow. This kind of problem is avoided by imposing the so called *Delaunay condition* to the simplicial complex: the circle passing through the vertices of a triangle must not contain any vertex of any other triangle of the complex. It may be noted that this condition is met for the circle passing through the vertices of γ (and of the other primal cells in Fig. 1). In this way we obtain dual cells (suitable for balance equations) such as the shaded polygon of Fig. 1. A dual mesh associated to a Delaunay network is named *Voronoy tessellation* and every vertex of the primal complex is inside a unique dual cell. For instance, V in Fig. 1 is inside the shaded dual cell. It is also closer to any point inside the shaded cell than any other vertex of the (primal) Delaunay network. This property leads to the concept of *area of influence* and suggests the idea of deriving an equilibrium equation for each dual cell [10].

Solution of elastic-plastic problems

As pointed out before, we assume a homogeneous deformation within each primal cell. The components of the strain tensor \mathbf{e}_α concerned with one cell (say α) depend upon the

horizontal displacements u_i, u_j, u_k and on the vertical displacements v_i, v_j, v_k of the vertices P_i, P_j, P_k (cf. Fig. 3). We obtain:

$$\epsilon_{xx} = (1/2A) \{-(y_j - y_i) u_k - (y_k - y_j) u_i - (y_i - y_k) u_j\}, \quad (1a)$$

$$\epsilon_{yy} = (1/2A) \{(x_j - x_i) v_k + (x_k - x_j) v_i + (x_i - x_k) v_j\}, \quad (1b)$$

$$\epsilon_{xy} = (1/4A) \{-(y_j - y_i) v_k + (x_j - x_i) u_k - (y_k - y_j) v_i + (x_k - x_j) u_i - (y_i - y_k) v_j + (x_i - x_k) u_j\} \quad (1c)$$

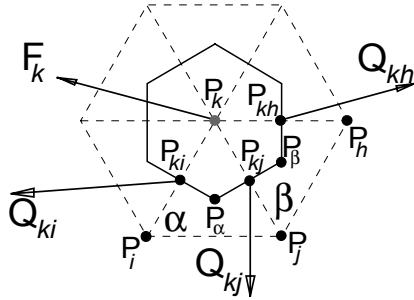


Fig. 3 - Internal dual cell

In the above equations A_α is the cell area, while x and y denote vertex coordinates. Thus, the equilibrium equation concerned with the k -th dual cell reads

$$\mathbf{Q}_{kj} + \mathbf{Q}_{kh} + \dots + \mathbf{Q}_{ki} + \mathbf{F}_k = \mathbf{0}, \quad (2)$$

where \mathbf{F}_k is the relevant body force, while the vectors $\mathbf{Q}_{kj}, \mathbf{Q}_{kh}, \dots, \mathbf{Q}_{ki}$ denote interface forces.

Each force (say \mathbf{Q}_{kj} , related to the interface $P_\alpha P_\beta$) depends upon the stress tensors $\mathbf{s}^{*,\alpha}$ and $\mathbf{s}^{*,\beta}$ of the primal cells (α and β) whose circumcentres are P_α and P_β (cf. Fig. 3). Thus, we can set

$$\mathbf{Q}_{kj} = \mathbf{s}^{*,\beta} \mathbf{R} (P_{kj} - P_\beta) - \mathbf{s}^{*,\alpha} \mathbf{R} (P_{kj} - P_\alpha), \quad (3)$$

where \mathbf{R} represents the (90 degree) rotation tensor

$$\mathbf{R} = \begin{bmatrix} 0 & -1 \\ 1 & 0 \end{bmatrix}. \quad (4)$$

Slightly different relationships are needed in the case of boundary cells. Thus, eqn. (2) becomes (cf. Fig. 4)

$$\mathbf{Q}_{kj} + \mathbf{Q}_{kh} + \dots + \mathbf{Q}_{ki} + \mathbf{F}_k + \mathbf{F}_B = \mathbf{0}, \quad (5)$$

where \mathbf{F}_B refers to boundary forces. The loads acting upon interfaces between contiguous dual cells can be expressed again through equations such as (3). However, we shall impose $\mathbf{s}^{*,\alpha} = \mathbf{0}$ or $\mathbf{s}^{*,\beta} = \mathbf{0}$ when the interface belongs to a single cell of the primal network.

By introducing the elastic stiffness tensor \mathbf{D}_α , we can set

$$\mathbf{s}_\alpha = \mathbf{D}_\alpha \mathbf{e}_\alpha. \quad (6)$$

Then, we can write eqn. (2) for each dual cell and express the terms \mathbf{Q}_{kj} in (3) as functions of convenient displacements by means of eqns. (6) and (1). Eventually, we obtain the linear system

$$\mathbf{K} \mathbf{U} = \mathbf{F}. \quad (7)$$

In the above equation, \mathbf{U} and \mathbf{F} collect displacement and force components, respectively. The matrix \mathbf{K} is fully analogous to the stiffness matrix of discrete finite element models and is symmetric, positive definite for properly constrained systems. Indeed, \mathbf{K} does coincide with the corresponding finite element matrix if 3-node elements analogous to the primal cells are selected. It is clear, however, that the theoretical background utilised in this context is completely different. In addition, equilibrium is not satisfied by considering (fictitious) point forces, such as equivalent nodal loads, but by focusing on loads that are actually exchanged along interfaces and, in principle, can be measured by means of appropriate devices (*e.g.*, flat jacks).

Eqn. (7) allows one to solve linear elastic problems. Minor manipulations, also provide relationships that are suitable for the solution of elastic plastic problems. In this case the constitutive equation (6) is substituted by the relationship

$$\mathbf{s}_\alpha = \mathbf{D}_\alpha \{ \mathbf{e}_\alpha - \mathbf{w}_\alpha \}, \quad (8)$$

where \mathbf{w}_α is the plastic strain tensor. Thus, eqn. (7) becomes

$$\mathbf{K} \mathbf{U} + \mathbf{L} \mathbf{W} = \mathbf{F}, \quad (9)$$

where \mathbf{W} collects all the independent components of the strain tensors \mathbf{w}_α , while \mathbf{L} is a constant matrix that transforms inelastic strains into convenient loads. Eventually, eqn. (9) and a proper yield condition can lead to the numerical solution of elastic plastic problems [11].

Applications to crack growth problems

The above framework can be applied to the study of quasi-brittle fracture, by assuming that the interfaces of the Voronoy network represent a discrete set of possible paths suitable for crack propagation. The basic idea is that a convenient criterion (*e.g.*, Coulomb's condition) may be utilised in order to find the loads under which a potential crack surface becomes active.

The easiest way of implementing the technique may be described as follows.

The average force acting on each interface, say \mathbf{Q}_k , is considered, with $k=1, \dots, n_V$, if n_V denotes the total number of interfaces of Voronoy's network. Next, we impose that the shear component Q_t and the normal component Q_n satisfy the selected condition. The most obvious example is provided by the classical inequality

$$|Q_t| \leq Q_c - Q_n \tan \varphi, \quad (10)$$

where Q_c and φ depend upon the material and the interface area. In the above equation, normal loads Q_n are clearly negative if they denote compression forces.

As typical with nonlinear problems, the numerical solution can be found by subdividing the load history into a finite number of time steps. Next, displacement increments are determined at each step by using an iterative procedure. The iterative process can be summarised as follows:

- Initial displacements, stresses and interface forces $\{\Delta Q^o\}_k$ are given at the beginning of each step
- Eqn. (9) is written in the form

$$\mathbf{K} \Delta \mathbf{U} = \Delta \mathbf{F} + \Delta \mathbf{F}^*, \quad (11)$$

and $\Delta \mathbf{F}^*$ (vector of interface forces due to possible inelastic deformations) is set equal to zero at the first iteration

- Incremental displacements $\Delta \mathbf{U}$ are found by means of eqn. (11)
- Incremental interface forces $\{\Delta Q^E\}_{ks}$ are computed (forces that would occur if the response to $\Delta \mathbf{U}$ were fully elastic) and interface forces

$$\mathbf{Q}_k = \{\mathbf{Q}^o\}_k + \{\Delta \mathbf{Q}^E\}_k - \{\Delta \mathbf{Q}^*\}_k, \quad (12)$$

are determined, whose components Q_n and Q_t satisfy the required condition

- A new vector $\Delta \mathbf{F}^*$ is determined that collects the forces $\{\Delta \mathbf{Q}^*\}_k$
- Eqn. (11) is solved again by using the updated vector $\Delta \mathbf{F}^*$ and the iterative process continues until the difference between the norms of $\Delta \mathbf{F}^*$ computed at two subsequent iterations does not exceed a given tolerance.

As pointed out above, the forces $\Delta \mathbf{F}^*$ are due to inelastic effects and must satisfy an appropriate condition. In this context, even if the final object is the study of crack propagation, fracture processes are not explicitly described by displacement discontinuities. On the contrary, their effects are simulated by assuming inelastic strains in zones located around the interfaces. For instance, such zone may be the one shown by a thick line in Fig. 5. Thus, proper values of $\{\Delta \mathbf{Q}^*\}_k$ are found by introducing fictitious, relative displacements δ and η at the interface (along the normal and the tangential

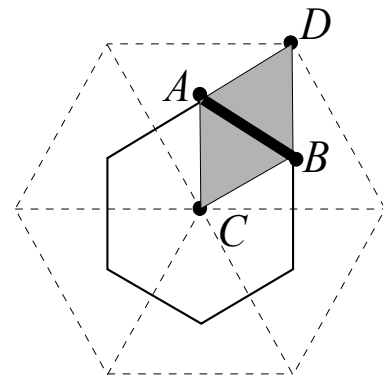


Fig. 5 - Cracked surface

direction) and by setting

$$Q_n = \{Q^\circ\}_n + \{\Delta Q^E\}_n - (S/L^*) D_{nn} \delta - (S/L^*) D_{nt} \eta \quad (13a)$$

$$Q_t = \{Q^\circ\}_t + \{\Delta Q^E\}_t - (S/L^*) D_{tn} \delta - (S/L^*) D_{tt} \eta, \quad (13b)$$

where D_{pq} ($p, q = n$ or t) are entries of the material stiffness matrix, S represents the area of the interface and L^* denotes the neighbourhood thickness. If both sides of eqns. (13) are divided by S , we obtain the relationships

$$\sigma_n = (\sigma^\circ)_n + (\Delta\sigma^E)_n - D_{nn} \varepsilon^i - D_{nt} \gamma^i, \quad \tau = \tau^\circ + \Delta\tau^E - D_{tn} \varepsilon^i - D_{tt} \gamma^i, \quad (14a,b)$$

subject to the constraint imposed by the selected condition. An easy example is given by the inequality (10) to be satisfied by $Q_t = \tau S$ and $Q_n = \sigma S$. Clearly, in this case a convenient ratio between the inelastic strains ε^i and γ^i must be introduced (e.g., $\varepsilon^i/\gamma^i = \pm \tan \varphi$).

The displacements δ and η (related to crack opening) affect the relative displacement of the points C and D in Fig. 5. Note that the same relative displacement may be obtained by a uniform distribution of inelastic strains ε^* and γ^* in the shaded quadrangle $ADBC$. Such strains must satisfy the conditions $\varepsilon^i L^* = \varepsilon^* L_{CD}$ and $\gamma^i L^* = \gamma^* L_{CD}$, where L_{CD} is the length of the segment CD in Fig. 5.

The above remark, also suggests a different way of using the *smear*d crack concept (inelastic strains instead of actual displacement discontinuities). Indeed, each triangle of the Delaunay network can be divided into three small triangles (Fig. 6), in which uniform inelastic strains are assumed. Thus, we can make use of eqn. (8), by assuming that α refers to a small triangle inside one primal cell ($\alpha = 1, \dots, 3c_p$, if c_p is the total number of primal cells). Next, an equation such as (9) can be derived and we can set $\Delta \mathbf{F}^* = -\mathbf{L} \Delta \mathbf{W}$ (as we do for any traditional elastic-plastic analysis). Obviously, the vector $\Delta \mathbf{W}$ will contain $3c_p$ subvectors $\{\Delta \mathbf{w}^*\}_\alpha$ (subvectors that collect the independent components of the strain tensors $\Delta \mathbf{w}_\alpha$). Each inelastic strain tensor $\Delta \mathbf{w}_\alpha$ will be associated to a fracture process that takes place along the portion of the interface that belongs to the α -th small triangle (e.g., segment AB in Fig. 6).

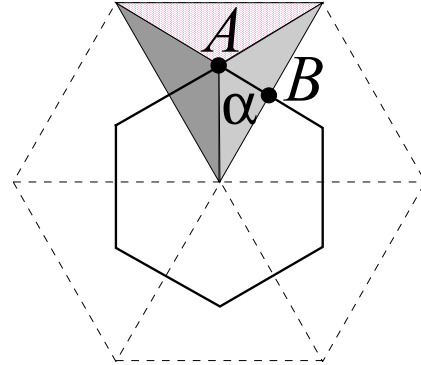


Fig. 6 - Small triangular regions

In any case, the model discussed here implies crack effects smeared throughout a certain volume element. As already pointed out, when the relative displacement d between two points (e.g., C and D in Fig. 5) is partially due to crack opening, the portion of d related to inelastic effects is given by ϵ^*L^* , where ϵ^* is one strain component and L^* a characteristic length. This fact must be considered when a softening law is defined. First, for any interface we need a critical tensile stress σ_c at which inelastic effects start to occur (Fig. 7). Next, a critical inelastic strain ϵ_c must be defined at which the tensile stress becomes zero. Taking into account

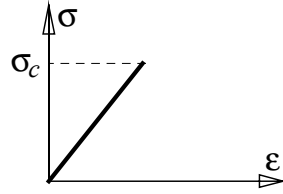


Fig. 7 - Linear σ - ϵ plot

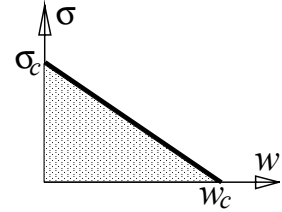


Fig. 8 - σ - w plot

the features of the smeared crack model, ϵ_c must be defined in such a way that $w_c = \epsilon_c L^*$, where w_c denotes the critical crack opening at which σ becomes zero (Fig. 8). In this way, when the inelastic strain computed according to the smeared crack model becomes equal to ϵ_c , a fracture energy has been released that corresponds to the shaded area in Fig. 8. This relation between critical strains and characteristic dimensions of the primal cells also allows one to remove, at least to some extent, mesh dependent results [12], which are quite typical in the presence of softening materials.

The nonlinear behaviour can be described by introducing a piecewise linear limit surface. An example is given in Fig. 9. Here the elastic domain is bounded by six lines in the plane Q_n - Q_t . In view of the piecewise linear approximation, inelastic strains are found through an equation such as $\{\mathbf{w}^*\}_\alpha = \mathbf{m}_\alpha \mathbf{z}_\alpha$, where \mathbf{z}_α contains six plastic multipliers (one for each line) and \mathbf{m}_α is a matrix of direction cosines.

Let us now introduce the vector $\mathbf{P}_j = \mathbf{D}_j \mathbf{A}_j (\{\mathbf{e}^*\}_j - \{\mathbf{w}^*\}_j)$ with $j=1, \dots, n_S$. The parameter n_S denotes the total number of segments AB (interfaces or half interfaces) to be considered, while the vector \mathbf{e}^*_{*j} collects the independent components of the strain tensor \mathbf{e}_j . The scalar quantity $A_j = t_j L_j$ is the area of the current full interface or half interface (product between its thickness and its length), while $[\mathbf{D}^*]_j$ is the stiffness matrix of the critical zone where inelastic strains are smeared. According to our model, such zone may be a small portion around an interface (Fig. 5) or a small triangle inside one dual cell (Fig. 6). The vector \mathbf{P}_j can also be expressed in the incremental form $\mathbf{P}_j = \{\mathbf{P}^o\}_j + \mathbf{S}_j \{\Delta \mathbf{e}^*\}_j - \mathbf{S}_j \mathbf{m}_j \Delta \mathbf{z}_j$, where \mathbf{S}_j is the block diagonal matrix $\mathbf{S}_j = [\mathbf{D}^*]_j \mathbf{A}_j$. Thus, for each critical zone we obtain

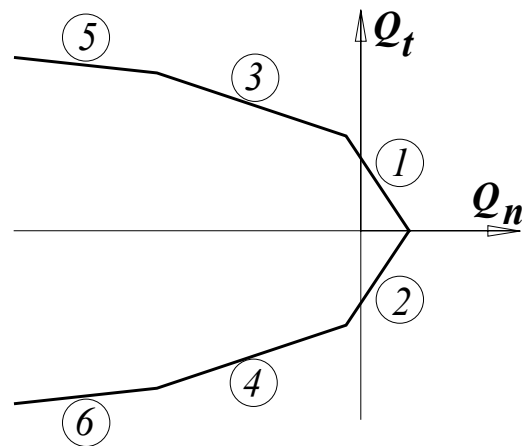


Fig. 9 - Piecewise-linear surface

$$\mathbf{y}_j = \{\mathbf{n}_j\}^T \{\mathbf{P}^\circ\}_j + \{\mathbf{n}_j\}^T \{\mathbf{S}_j \{\Delta \mathbf{e}^*\}_j - \mathbf{S}_j \mathbf{m}_j \Delta \mathbf{z}_j\} - \mathbf{r}_j \leq \mathbf{0} \quad , \quad \Delta \mathbf{z}_j \geq \mathbf{0} \quad , \quad \{\mathbf{y}_j\}^T \Delta \mathbf{z}_j = 0 \quad (15a,b,c)$$

Here, the vector \mathbf{r}_j gives the distances of the six lines in Fig. 9 from the origin. The matrix \mathbf{n}_j (made of outward unit vectors) is needed to project the stress vector along directions which are orthogonal to the six lines. In this way, active inelastic modes can be detected. Finally, the complementarity constraint (15c) allows inelastic strains to become non-zero when at least one yield locus is violated.

When the above conditions are satisfied for each critical zone, the constitutive law can be enforced in the framework of a nonlinear step-by-step analysis.

If \mathbf{r}_j remains constant throughout the load history, an elastic perfectly plastic behaviour is recovered. On the other hand, hardening and/or softening may be introduced by assuming a convenient function $\mathbf{r}_j = \mathbf{r}_j(\Delta \mathbf{z}_j)$. At present, we are considering a possible softening behaviour for planes 1 and 2 in Fig. 9.

One further enhancement of the structural response is possible by enforcing some loss of stiffness related to inelastic strains [13]. This feature has not been implemented, yet, in the framework of the discrete formulation discussed here.

As pointed out above, softening has been considered for planes 1 and 2 (Fig. 9), by assuming a relationship $r = r(z)$, such as the one represented in Fig. 10. It is characterised either by the single softening branch (a) or by the horizontal branch (b). This second branch is needed since the solution of the problem (15) obtained by using the branch (a) may lead to a negative value of $r = r(z)$. In this case, a new solution is found by using the branch (b). The r - z plot of Fig. 10 implies the relationship $\mathbf{r}_j = \{\mathbf{r}^\circ\}_j + \mathbf{H}_j \Delta \mathbf{z}_j$, with \mathbf{H}_j constant, and makes eqns. (15) define a linear complementarity problem [14, 15].

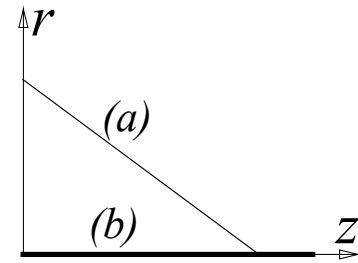


Fig. 10 - r vs. z plot

It is worth noting that the model is also able to describe crack closure.

To this aim we start by selecting the critical zones (full interface of Fig. 5 or half interface of Fig. 6) which have lost their tensile strength (zero distance of lines 1 and 2 from the origin). Next, for these zones we introduce a vector $\Delta \mathbf{z}_{0;j}$, whose non-zero entries may be the terms that correspond to the lines passing through the origin: sthey will be given the values attained by the multipliers at the end of the previous time step.

In order to take into account crack closure, we need to consider also each critical zone where a normal (positive) inelastic strains $\epsilon_{N;j}$ combined with a positive normal stress $\sigma_{N;j}$ has occurred at least once. If the tensile strength is not fully lost (no line passes through the origin), we introduce the parameter $(q^\circ)_j = (\epsilon^N)_j$, where $(\epsilon^N)_j$ denotes the current inelastic strains. We also define a new stiffness parameter $(h^*)_j = (\sigma^*)_j / (\epsilon^*)_j$, where $(\epsilon^*)_j$ is the largest value ever attained by $(\epsilon^N)_j$ and $(\sigma^*)_j$ is the corresponding (positive) normal stress.

After introducing the vector $\{\Delta \mathbf{z}^\circ\}_j$ and the parameter $q_{0;j}$, we may consider the problem [8]

$$\mathbf{y}_j = \{\mathbf{n}_j\}^T (\mathbf{P}^\circ)_j + \mathbf{n}^T \mathbf{S}_j \{\Delta \mathbf{e}_j + \mathbf{C} (q^\circ)_j + \mathbf{m}_j \{\Delta \mathbf{z}^\circ\}_j - \mathbf{C} q_j - \mathbf{m}_j \Delta \mathbf{z}_j\} - r_j \leq \mathbf{0} \quad (16a)$$

$$\Delta \mathbf{z}_j \geq \mathbf{0}, \quad \{\mathbf{y}_j\}^T \Delta \mathbf{z}_j = 0 \quad (16b,c)$$

$$\mathbf{v}_j = \mathbf{B} (\mathbf{P}^\circ)_j + \mathbf{B} \mathbf{S}_j \{\Delta \mathbf{e}_j + \mathbf{C} (q^\circ)_j + \mathbf{m}_j \{\Delta \mathbf{z}^\circ\}_j - \mathbf{C} q_j - \mathbf{m}_j \Delta \mathbf{z}_j\} - (h^*)_j q_j \leq \mathbf{0} \quad (16d)$$

$$q_j \geq \mathbf{0}, \quad \mathbf{v}_j q_j = 0 \quad (16e,f)$$

where $\mathbf{C}=[1 \ 0]^T$ transforms $q_{o,j}$ into a two-entry vector. Similarly, the matrix $\mathbf{B}=\mathbf{C}^T$ selects the entry of the vector \mathbf{P}_j , defined above, which represents the normal force associated to the strain component $(\epsilon^N)_j$.

When conditions (16) are satisfied, the normal inelastic strains are progressively recovered if the corresponding total strains decrease. In any case, the increments of the inelastic strains at the end of the current time step are given by $\{\mathbf{C} \mathbf{q} + \mathbf{m} \Delta \mathbf{z} - \mathbf{C} \mathbf{q}_o - \mathbf{m} \Delta \mathbf{z}_o\}$. It is worth noting that the problem (16) and eqn. (11), in which $\Delta \mathbf{F}^* = -\mathbf{L} \Delta \mathbf{W}$, generalise the governing equations

$$\sigma_o + k (\Delta \epsilon + \xi_o - \Delta \lambda - \xi) = \sigma, \quad \sigma - h \Delta \lambda - \sigma^* = y \leq 0, \quad \Delta \lambda \geq 0, \quad y \Delta \lambda = 0, \quad (17a,b,c,d)$$

$$\sigma - g \xi = v \leq 0, \quad \xi \geq 0, \quad v \xi = 0. \quad (17e,f,g)$$

These equations govern the response of the mechanical system shown in Fig. 11a. It is made of three linear elastic springs (whose stiffness parameters are $k, h < 0, g$), one rigid, perfectly plastic slip (with yield limit equal to σ^*) and one no-tension element characterised by reversible strains ξ [16]. The relevant σ - ϵ plot is given in Fig. 11b. Note that the dashed path in Fig. 11b is allowed by eqns. (17), not not by eqns. (16).

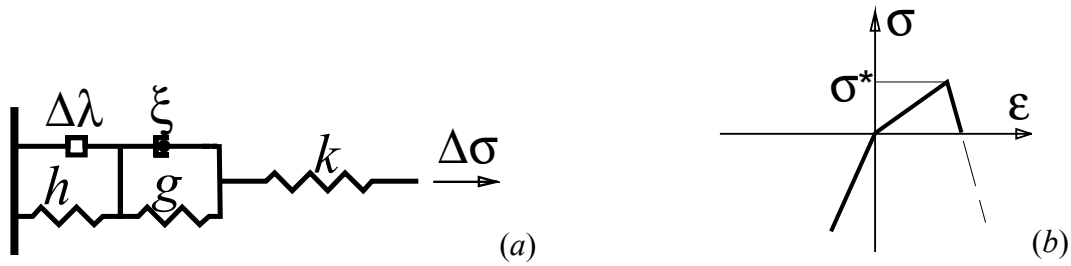


Fig. 11 - Mechanical model (a) and σ - ϵ plot (b)

Applications to masonry

The same concepts developed in the previous Sections may be applied to dual meshes made of rectangles. An example is given by Fig. 12, where thick lines refer to the *primal* mesh.

For each rectangle of the primal mesh (e.g., *ABCD* in Fig. 12) it is possible to assume a bilinear displacement field, that depends upon vertex displacements. Next, every rectangle is divided into four triangles (1, 8, 9, 10 in Fig. 13), where the displacement gradient and the relevant strain distribution can be determined. For the sake of simplicity, strain fields may be approximated by uniform distributions.

The triangles of Fig. 13 have the same functions of the three shaded triangles in Fig. 6.

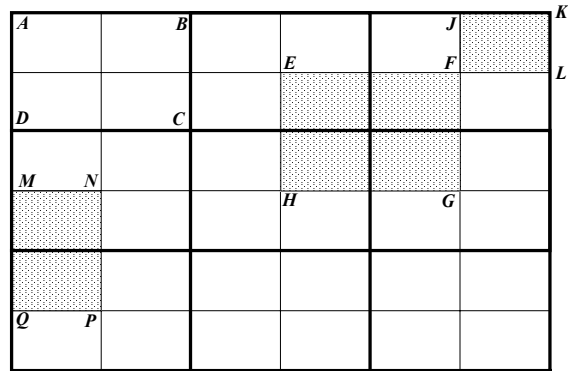


Fig. 12 - Primal and dual mesh

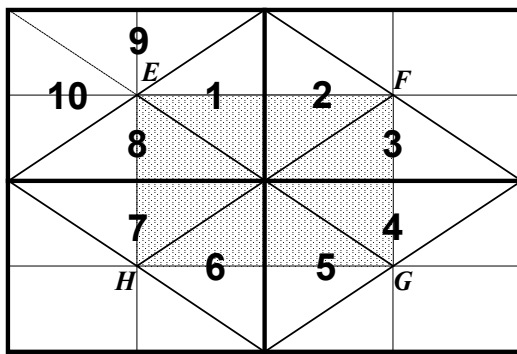


Fig. 13 - Dual cell subdivided into 8 triangles

along the interfaces of the primal cells (e.g., segments 1-8 in Fig. 13). This can be done by introducing a yield surface in the space N_x - N_y - S , where N_x or N_y are normal forces acting along one interface, while S denotes the corresponding shear load. For instance, Coulomb's criterion can be applied. In this case, a possible yield locus is the one shown in Fig. 9, where the six lines represent projections of yield surfaces in the plane Q_n - Q_t (instead of N_x - S or N_y - S).

The primal and dual meshes discussed in this Section are quite suitable for the numerical analysis of masonry. Indeed, masonry can be described as a macroscopically homogeneous material (without considering the mechanical properties of mortar and bricks or stones separately). For instance, the discrete system of Fig. 13 can be utilised for the masonry assembly of Fig. 14. In this case, it is assumed that joint slips may occur

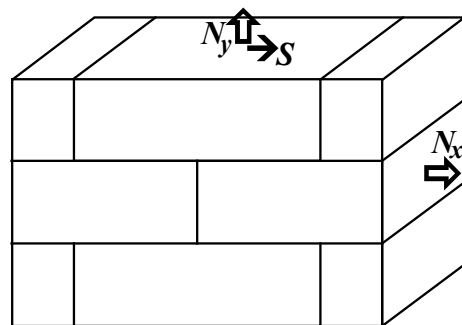


Fig. 14 - Typical brickwork

In the case of masonry, however, one further inelastic phenomenon should be considered. Indeed, fracture processes in bricks may occur. They can be described by introducing a convenient criterion at the vertical interfaces. To this aim, we have set some limitation to horizontal strains, by introducing an additional yield surface whose projection on the N_x - N_y plane is shown in Fig. 15 with a thick line. The thin line has no interest in this context, since it refers to values of N_x and N_y for which horizontal cracks (detachments parallel to mortar beds) would start to develop.

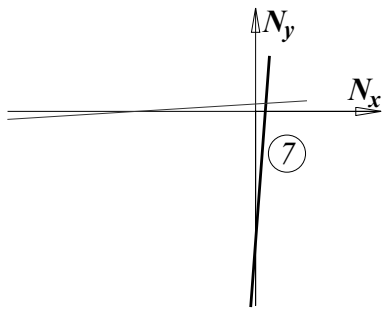


Figure 15: Yield plane 7

Eventually, the model implies a small number of possible failure modes (slips or cracks at joints and vertical cracks in bricks). In spite of obvious limitations, this choice seems to be a reasonable compromise between the advantages of a simple description and a satisfactory level of accuracy. Indeed, the model appears suitable for practical applications, since limited experimental information is required: joint strength and critical brick elongation. Such parameters can be estimated, at least to some extent, even in the case of historical monuments.

Numerical tests

Some characteristic results are shown in Figs. 16 and 17. The first picture is concerned with one mortar specimen subject to compression. The typical hour-glass shape after collapse can be noted, since black segments denote cracked areas. Note that the length of each segment is proportional to the norm of the inelastic strain vector that occurs in the region around the relevant interface. Fig. 17 is referred to a notched concrete beam subject to four point bending. As before, black lines show the presence of cracks. Figs. 16 and 17 were clearly obtained by using Delaunay's network as primal mesh and, hence, Voronoy's tessellation as dual mesh (combined with an appropriate algorithm for the detection of inelastic strains). Finally, Fig. 18 shows one plot related to the response of a masonry shear wall subject to cyclic loads [8].

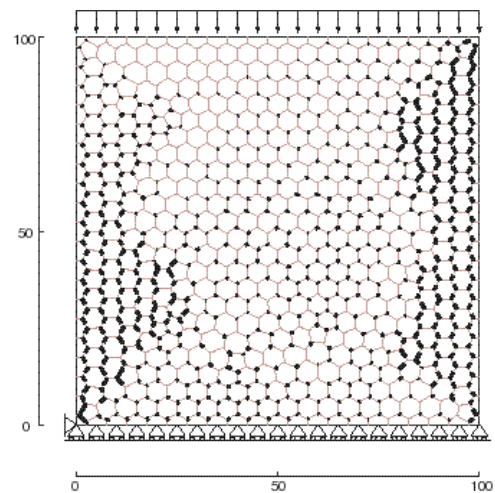


Fig. 16 - Mortar specimen

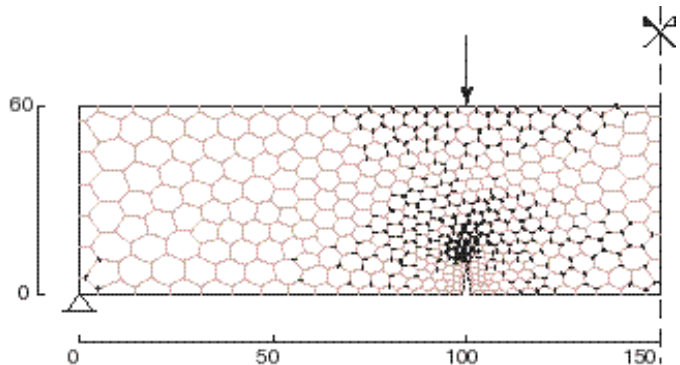


Fig. 17 - Notched beam subject to bending

In this case, rectangular cells (as discussed in the previous Section) were utilised for the primal and the dual mesh. First, the bottom edge was constrained and vertical downward uniform displacements were imposed along the upper edge in order to induce compression. Next, a cyclic uniform horizontal displacement was applied to the top edge and the relevant shear is reported as function of such displacement (thin line). Owing to the load condition selected for this sample problem, joint cracks in the central region were the main inelastic effects in the wall. The thick curve gives the computed response when the displacements applied along the top edge increase monotonically.

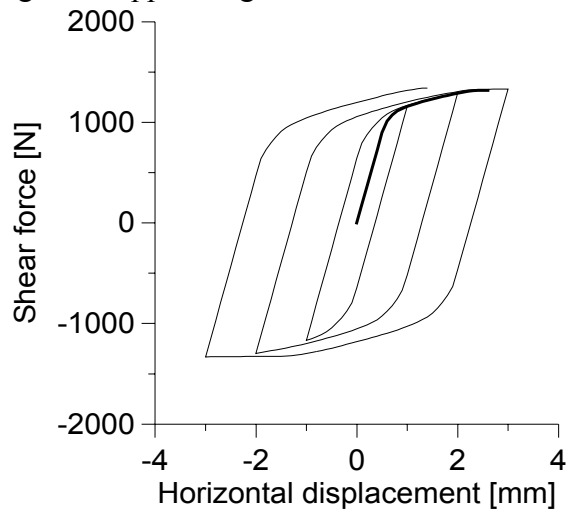


Fig. 18 - Response of a shear wall

Acknowledgements

The financial support of the Italian Ministry of University and Scientific Research is acknowledged.

References

- [1] Tonti E., On the mathematical structure of a large class of physical theories, *Rendiconti Acc. Lincei - Serie VIII*, **52**, 1972, 48-56
- [2] Tonti E., A mathematical model for physical theories, Part I, *Rendiconti Acc. Lincei - Serie VIII*, **52**, 1972, 175-181
- [3] Tonti E., A mathematical model for physical theories, part II, *Rendiconti Acc. Lincei - Serie VIII*, **52**, 1972, 350-356
- [4] Oden J.T. and Reddy J.N., *Variational methods in theoretical mechanics*, Springer-Verlag, Berlin, 1976.
- [5] Tonti E., On the geometrical structure of electro-magnetism, in: *Gravitation, electromagnetism and geometrical structures* (Ferrarese G. ed.), Pitagora Editrice, Bologna, 1997, 281-308
- [6] Barenblatt G.I., The mathematical theory of equilibrium cracks in brittle fracture, *Adv. Appl. Mech.*, **7**, 1962, 55-129
- [7] Hillerborg A., Mod er M. and Pettersson P.E., Analysis of crack formation and crack growth in concrete by means of fracture mechanics and finite elements, *Cement Concrete Res.*, **6**, 1976, 773-782
- [8] Nappi A. and Tin-Loi F., A discrete formulation for the numerical analysis of masonry structures, in: *Proc. Fourth Asia-Pacific Conference on Computational Mechanics*, Singapore, 15-17 December 1999, to appear
- [9] Mattiussi C., An analysis of finite volume, finite element, and finite difference methods using some concepts from algebraic topology, *J. Comput. Phys.*, **133**, 1997, 289-309

- [10] Tonti E., A discrete formulation for the wave equation, in: *Proc. ICTCA '99*, Trieste, Italy, 10-14 May 1999, to appear
- [11] Nappi A., Rajgelj S. and Zaccaria D., Application of the cell method to elastic-plastic analysis, in: *Physics and mechanics of finite plastic & viscoplastic deformation* (Khan A.S. ed.), Neat Press, Md, 433-434, 1999
- [12] Bazant Z.P. and Cedolin L., Blunt crack band propagation in finite element analysis, *J. Eng. Mech. (ASCE)*, **105**, 297-315, 1979
- [13] Nappi A., Facchin G. and Marcuzzi C., Structural dynamics: convergence properties in the presence of damage and applications to masonry structures, *Structural Engineering and Mechanics*, **5:5**, 587-598, 1997
- [14] Maier G., A matrix structural theory of piecewise-linear plasticity with interacting yield planes, *Meccanica*, **5:1**, 1970, 55-66
- [15] Cottle R.W., Pang, J.S. and Stone, R.E., *The linear complementarity problem*, Academic Press, 1992
- [16] Nappi A., Facchin G. and Rajgelj S., Boundary element algorithms for elastic-plastic analysis: an extension to describe damage effects, *Engineering Analysis with Boundary Elements*, **14**, 1994, 15-24